Composites

CrossMark

Microstructure and mechanical behaviour of aluminium matrix composites reinforced with graphene oxide and carbon nanotubes

Paloma Hidalgo-Manrique[1], Shaojiu Yan[2,*], Fei Lin[1], Qihu Hong[2], Ian A. Kinloch[1], Xiang Chen[2], Robert J. Young[1,*] (iD), Xiaoyan Zhang[2], and Shenglong Dai[2]

[1] *National Graphene Institute and School of Materials, University of Manchester, Manchester M13 9PL, UK*
[2] *Beijing Institute of Aeronautical Materials (BIAM), Beijing, China*

ABSTRACT

Aluminium (Al) matrix composites reinforced with either 0.5 wt% graphene oxide (GO) or 0.5 wt% carbon nanotubes (CNTs) were hot extruded from ball-milled powders. A control, pure Al bar was also fabricated. Microstructural examination, including Raman mapping, showed a relatively poor dispersion of the carbon nanomaterials within the Al matrix, particularly in the case of the CNTs. Consequently, while the mean grain size of the Al matrix remains invariant with the addition of CNTs, the Al/GO composite exhibits reduced grain size compared to pure Al due to the pinning effect of the reinforcement. Moreover, the addition of both carbonaceous materials resulted in a slight decrease in the typical extrusion duplex <111> + <100> fibre texture intensity. This weakening of the texture was more pronounced in the Al/GO composite, partly due to the pinning effect of the reinforcement. In agreement with their relative mean grain sizes, the Al/GO composite shows an improved mechanical performance over pure Al. Despite the similarity of the mean grain sizes, the Al/CNT composite displays comparable hardness and a decreased compressive yield stress relative to the pure Al. In the absence of chemical reactions at the interfaces, this was attributed to a low efficiency of load transfer from the Al matrix to the reinforcement resulting from the large extent of agglomeration of CNTs.

Introduction

Aluminium (Al) is currently the leading non-ferrous metal in use due to its combination of exceptional properties, including low density, excellent corrosion resistance, suitability for surface treatments, good formability, high recyclability and large availability. The transportation industry accounts for the largest share of Al consumption, with Al being the primary material of choice for structural components in

Address correspondence to E-mail: shaojiuyan@126.com; robert.young@manchester.ac.uk

aircraft throughout most of its history [1, 2]. There has recently been a strong demand for Al products with improved mechanical properties [3]. This is in order to meet the ever-increasing service requirements of airplanes and spacecraft [4] as well as the growing need to reduce the weight of vehicles such as cars, trains or ships and thus their impact on the environment, but without reducing the occupant safety. It is difficult, however, to achieve significant improvements in the mechanical performance of Al products using the conventional approaches based on alloy chemistry, heat treatments and deformation [5].

Aluminium matrix composites (AMCs) typically exhibit improved specific strength and stiffness compared to the Al metal matrices due to reinforcement from non-metallic phases [6–8]. Actually, the composite approach is the only way to enhance the Yong's Modulus of metals and alloys. In addition, AMCs also exhibit higher wear, creep and fatigue resistance, the mechanical properties depending on the reinforcement content, size, shape and distribution [7, 8] and on the characteristics of the reinforcement/matrix interface [6]. For this reason, despite the ductility and toughness reduction often seen in conventional AMCs [8, 9], they are increasingly applied as structural materials in the ground transportation (auto and rail) and aerospace [7, 10]. Moreover, metal matrix composites (MMCs) offer a rich and vast playground for extending the application range of metals, owing to their unique balance of mechanical properties and physical properties that are inaccessible for metals and alloys [11]. Hence, AMCs, especially the particulate-reinforced composites, are of interest for certain functional applications, such as sub-components in aerospace systems, due to their appropriate coefficient of thermal expansion [7, 8].

The most common reinforcement materials in commercial applications include carbides (e.g. SiC, B_4C), nitrides (e.g. Si_3N_4, AlN), oxides (e.g. Al_2O_3, SiO_2), as well as elemental materials (e.g. C, Si) [6, 7]. The reinforcements may be in the form of continuous fibres, chopped fibres, whiskers, platelets, films or particulates [6], nearly all MMCs in commercial use relying on discontinuous reinforcements, which provide improved affordability and isotropy [7]. The size of such reinforcements has a strong effect on the strength and ductility of resulting composites. For the metal-based composites reinforced with ceramic particles or fibres, both the strength and ductility decrease with the increase in particle size [8, 12].

Hence, the mechanical performance of AMCs could be further increased by reducing the size of the reinforcements from the micrometre to the nanometre scale to form "nanocomposites". To date, various types of nanocrystalline materials have been developed recently so that nanomaterials with unique properties show great potential for use as reinforcing phases for metals [12, 13].

In recent years, carbonaceous materials including one-dimensional carbon nanotubes and two-dimensional graphene have emerged as an important class of new materials for structural engineering and functional device applications due to their extraordinarily high elastic modulus (1 TPa) and mechanical strength (up to 130 GPa, typically >10 GPa) as well as excellent electrical and thermal conductivities. In combination with their aspect ratio (i.e. length-to-thickness or length-to-diameter ratio) characteristics, graphene and carbon nanotubes are considered to be the most promising reinforcing fillers for fabricating composite materials [14]. However, considering the fact that most of the structural materials used in today's world are metals, it is quite surprising that, despite there having been a marked increase in the number of publications on the topic since 2003, the number of studies on reinforcement of metals by carbonaceous materials is still very low compared to their polymer composite counterparts [15]. This is due to the fact that the introduction of carbonaceous materials into the metal matrix is rather difficult due to the harsh fabrication conditions employed for processing composite materials (i.e. high temperature and high pressure). The main challenges in fabrication include obtaining a homogeneous dispersion of reinforcements within the matrix, the formation of strong interfacial bonding and the retention of the structural stability of the reinforcements [12, 13]. The processing technique plays a very important role in this regard. Powder metallurgy is, by far, the most feasible and widely used route for preparing MMCs reinforced with carbonaceous materials due to a superior balance of properties, modest cost and commercial availability in range of semi-finished products [7, 15].

This investigation was aimed at studying the effect of adding carbonaceous materials on the microstructure, texture and mechanical properties of an Al matrix. With this purpose in mind, pure Al was reinforced with 0.5 wt% graphene oxide (GO) and 0.5 wt% carbon nanotubes (CNTs) through a simple

powder metallurgy route combined with hot extrusion. After preparation, the matrix grain structure and crystallographic orientations as well as the dispersion of the reinforcing materials in the Al matrix of the composites were investigated and compared to the unreinforced material. The role of the pinning effect of the reinforcing materials, determined by their degree of agglomeration within the Al matrix, upon the resultant microstructure and texture of the composite materials was analysed. Hardness and compression tests were performed on both the Al/GO and Al/CNTs composites and the pure Al bar. The mechanical performance of the composites was interpreted in terms of the matrix grain size refinement and the effectiveness of the load transfer from the matrix to the reinforcements. The potential occurrence of interfacial reactions and the structure of the reinforcing materials in the composites were also evaluated.

Experimental procedure

The starting materials in this study were pure Al powders with an average particle size of 48 ± 18 μm as well as GO and CNTs powders. The Al/0.5 wt% GO and Al/0.5 wt% CNTs were prepared in a number of steps. Firstly, the Al and reinforcement powders were mixed by ball milling for 20 h at 70 rpm with a ratio of ball-to-material of 10:1. Afterwards, the mechanically mixed powders were green compacted under a pressure of 500 MPa at room temperature. Finally, the green compact was sintered at 600 °C for 2 h followed by hot extrusion at 420 °C to obtain bars of 12 mm in diameter. The ram speed was 20 mm/s and the extrusion ratio 16:1. The rods produced were then air-cooled. For comparison purposes, a pure Al bar was also prepared from the Al powders in the same manner.

Microstructural examinations were performed by means of scanning electron microscopy (SEM) in a Zeiss Sigma 99 equipped with a VP field emission gun. Electron backscatter diffraction (EBSD) was also carried out using a Sirion field emission gun scanning electron microscope (FEG-SEM) with a HKL EBSD system attached operated at 20 kV, using a sample tilt angle of 70° and a working distance of 16 mm. For orientation mapping, a step size of 0.05–0.1 μm was used. The EBSD analyses were completed using the commercially available HKL Channel 5 software.

The macrotexture was analysed by X-ray diffraction (XRD). The (111), (200), (220), (311) and (222) pole figures were measured using Cu K$_\alpha$ radiation in a Bruker D8 Discover diffractometer. From these experimental data, the orientation distribution function and the calculated pole figures were obtained using the MATLAB toolbox MTEX. XRD analysis was also performed to evaluate the presence of any carbides at the interfaces between the Al matrix and the reinforcements. For this purpose, a PANalytical X'Pert Pro diffractometer using a X'Celerator detector with a Cu K$_\alpha$ radiation source was employed. The 2θ angle ranged from 5° to 90° with a step of 0.03°.

Raman spectroscopy was conducted on the materials using a Renishaw system 1000 Raman spectrometer with 514 nm Ar$^+$ laser and a Renishaw System 2000 Raman spectrometer with 633 nm HeNe laser. Polarised Raman spectroscopy was undertaken by rotating the specimen in the spectrometer on a rotation stage while there was a polariser in the detector parallel to the incident laser polarisation. A Renishaw inVia Raman system with 633 nm HeNe laser was used to obtain the dispersion of fillers by Raman mapping. Calibration was undertaken for each spectrometer using the Si Raman band at 520 cm^{-1}.

The mechanical behaviour of the materials fabricated was evaluated by undertaking both hardness and compression testing at room temperature. Vickers microhardness tests were performed using a Struers Duramin indenter with a load of 1.96 N for 10 s. Uniaxial compression tests were conducted on a universal Instron machine at an initial strain rate of 10^{-3} s^{-1}. The tests were performed using lubrication in order to minimise friction between the sample and the anvils. Compression cylinders of 3 mm in diameter and 4.5 mm in height were machined from the extruded bars with their loading axis parallel to the extrusion direction (ED). The load–displacement data from the load frame were corrected for machine compliance and then used to calculate true stress (σ) and true strain (ε). The yield stress corresponding to each test was calculated as the true stress at 0.2% engineering strain. In addition, the work hardening rate (θ) was calculated as the slope of the σ–ε curves at each strain level.

The preparation of the bulk fabricated materials for SEM, EBSD, XRD, Raman and hardness analyses involved standard grinding with progressively finer SiC papers and subsequent polishing down to 1 μm with diamond pastes. Afterwards, the specimens for

SEM, EBSD and Raman inspections were additionally polished in colloidal silica. All the analyses were performed on regions close to the centre of the extruded bars. Finally, the initial GO and CNTs powders were dispersed in distilled water and ethanol with sonication followed by vacuum drying for Raman analysis.

Results

Microstructure

Backscattered electron SEM micrographs from sections perpendicular to the ED of the Al/GO and Al/CNT composites are displayed in Fig. 1. The micrographs show a relatively homogeneous grain size distribution for both composite materials. However, a homogeneous dispersion of carbon nanomaterials into the metal matrices is extremely difficult to achieve in fabricating composites because they tend to agglomerate into clusters during the composite processing in order to reduce their surface energy [12]. In fact, as shown in Fig. 1a, b, in the present composite materials reinforcements are poorly dispersed in the Al matrix and, despite the interfacial area being, in principle, higher for GO than for CNTs, agglomeration of reinforcement is especially evident in the Al/CNT composite. In this way, clusters of reinforcements (in black

contrast) are clearly observed in both materials, these being larger and showing a more heterogeneous spatial distribution in the Al/CNT composite. These clusters are preferentially located at the grain boundaries (GBs), corroborating the reported tendency for carbonaceous materials to distribute and agglomerate along the GBs [4, 11–13, 15–17]. The large degree of reinforcement agglomeration in the Al/GO (Fig. 2a) and Al/CNT (Fig. 2b) composites was further verified by Raman mapping on sections parallel to the ED (Fig. 2). In addition, the Raman maps reveal that the reinforcing materials tend to arrange in stringers aligned along the ED.

A close inspection of the composites by SEM (Fig. 1c, d) shows that both materials are also covered with nanoscaled white particles. The spatial distribution of these particles within the matrix is not uniform, their population being higher close to the reinforcement clusters. Moreover, in the regions without agglomerations they appear to decorate the GBs. Due to the easy oxidation of Al surfaces in air, these particles are identified as fractured alumina particles resulting from the extrusion process when the alumina layer that covers the Al particles breaks [18]. Owing to their small size, these particles could, to some extent, inhibit grain growth and thus contribute to the control the mean grain size of the pure Al and composite extrusions by pinning the GBs.
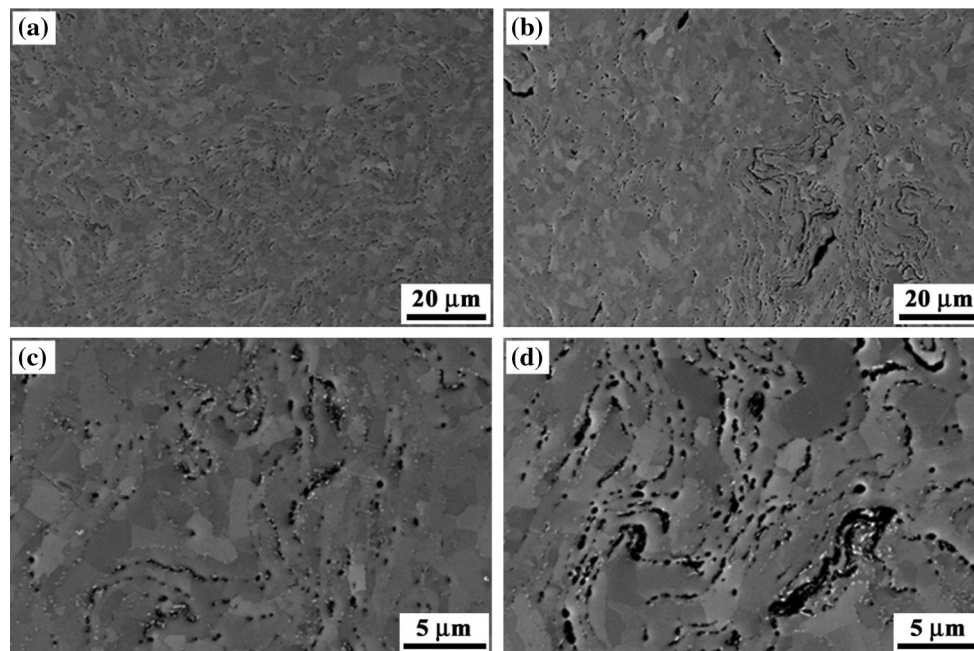

Figure 1 SEM micrographs from the transversal sections of the **a**, **c** Al/GO and **b**, **d** Al/CNT composites.
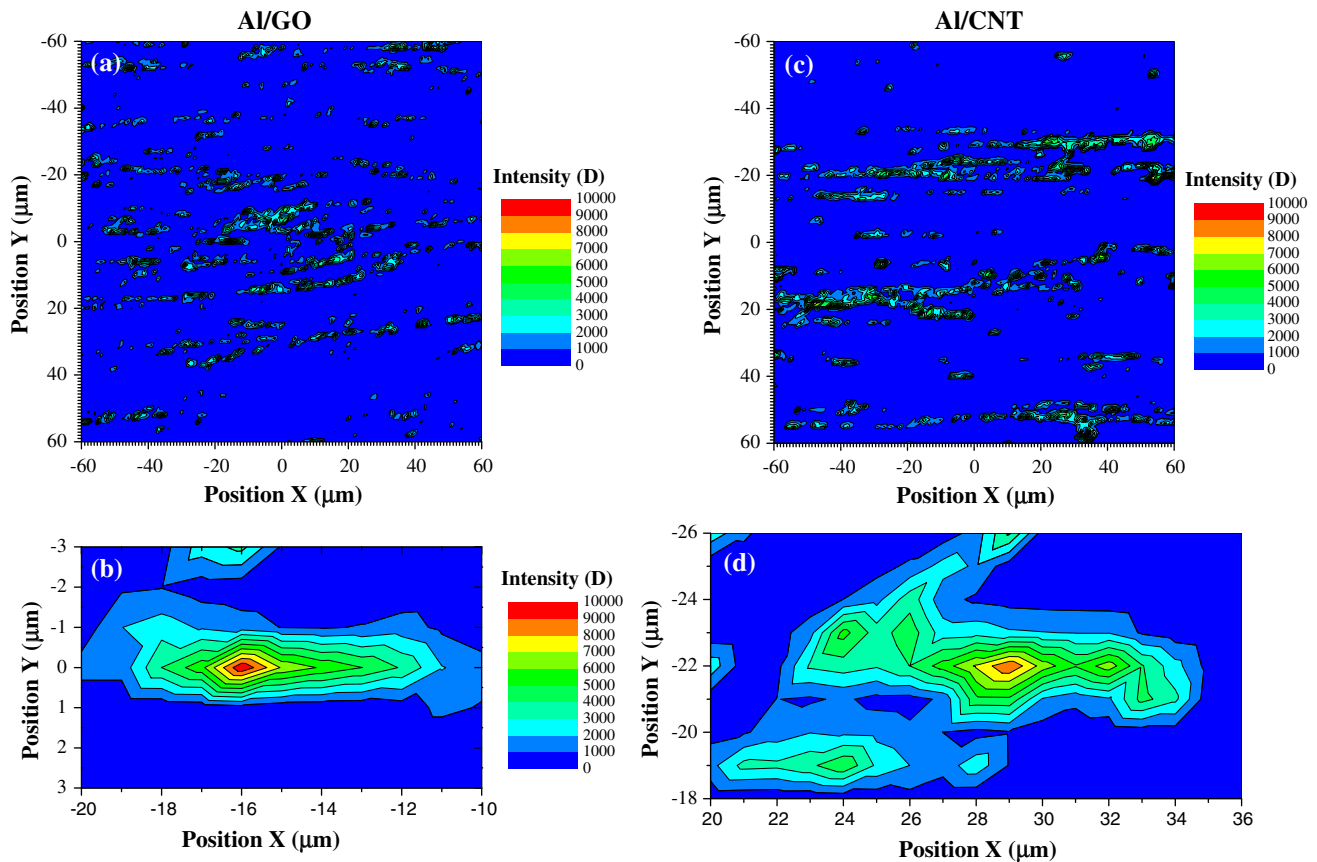
Figure 2 Raman maps showing the integrated intensity of the D band. **a** Al/GO composite at low magnification and **b** high magnification; **c** Al/CNT composite at low magnification and **d** high magnification. The extrusion direction is oriented approximately horizontal in the maps.

Figure 3 shows the EBSD maps from sections parallel to the ED of the pure Al bar and the Al/GO and Al/CNT composites. Boundaries with misorientations between 2° and 15° were defined as low-angle boundaries (LABs), while those with misorientations higher than 15° were defined as high-angle boundaries (HABs). The mean grain thickness (d_t), determined as the mean spacing of HABs along the direction perpendicular to the ED by using the linear intercept method, has been included in each map. It is clear that the three materials exhibit a microstructure composed of grains elongated along the ED with a homogeneous size. The microstructure of the Al/GO (Fig. 3b) composite is, however, finer than that of the unreinforced material (Fig. 3a) and the Al/CNT composite (Fig. 3c). Hence, the mean grain thickness has a value of around 1.55 μm for pure Al and the Al/CNT composite, but decreases to 0.72 μm with the additions of GO.

The fine grain size obtained for the present pure Al extruded bar proves the refinement potential of ball milling. This refinement is attributed to the intensive plastic deformation imposed on the material due to the strong deformation occurring in the collisions between the stainless steel balls and the Al powders and also to the pinning effect of the small alumina particles formed during the fabrication process [18, 19]. Since the fabrication conditions are the same for the three materials, the reduced grain size of the Al/GO composite compared with pure Al and the Al/CNT composite could be attributed to an additional pinning effect of GO, which despite the agglomeration is still capable to pin the GBs to some extent. On the contrary, the large degree of agglomeration of CNTs in the Al/CNT composite results in a negligible pinning effect, so that the mean grain size in this composite remains the same as that in the pure Al.
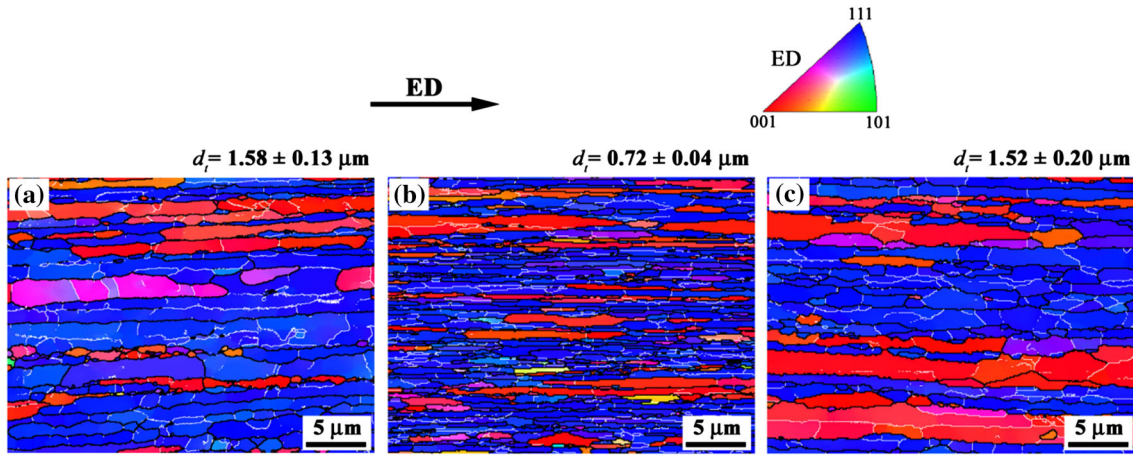
Figure 3 EBSD inverse pole figure maps in the extrusion direction (ED) of **a** the pure Al bar, **b** the Al/GO composite and **c** the Al/CNT composite. The mean grain thickness of each material has been included as an *inset*. The low-angle boundaries ($2° \leq \theta < 15°$) are depicted as *white lines*, while the high-angle boundaries ($\theta \geq 15°$) are depicted as *black lines*. The non-indexed points are shown as *black pixels*.

Texture

The colours in the EBSD maps (Fig. 3) represent the crystallographic orientations parallel to the ED. The correspondence between the colours and the crystallographic orientations is indicated in the stereographic triangle. The colours in the maps of the three materials suggest that, for a majority of the grains, the ED is close to the <111> or the <001> directions.

Detailed orientation data of the bulk for pure Al bar and the Al/GO and Al/CNT composites are plotted in {111} and {100} pole figures in Fig. 4. In agreement with the EBSD observations, the pole figures show that the three materials have a double fibre texture, with most of the grains having their <111> axis and some others having their <100> axis parallel to the ED. This is the common texture in extruded Al, the <111> fibre component corresponding to purely
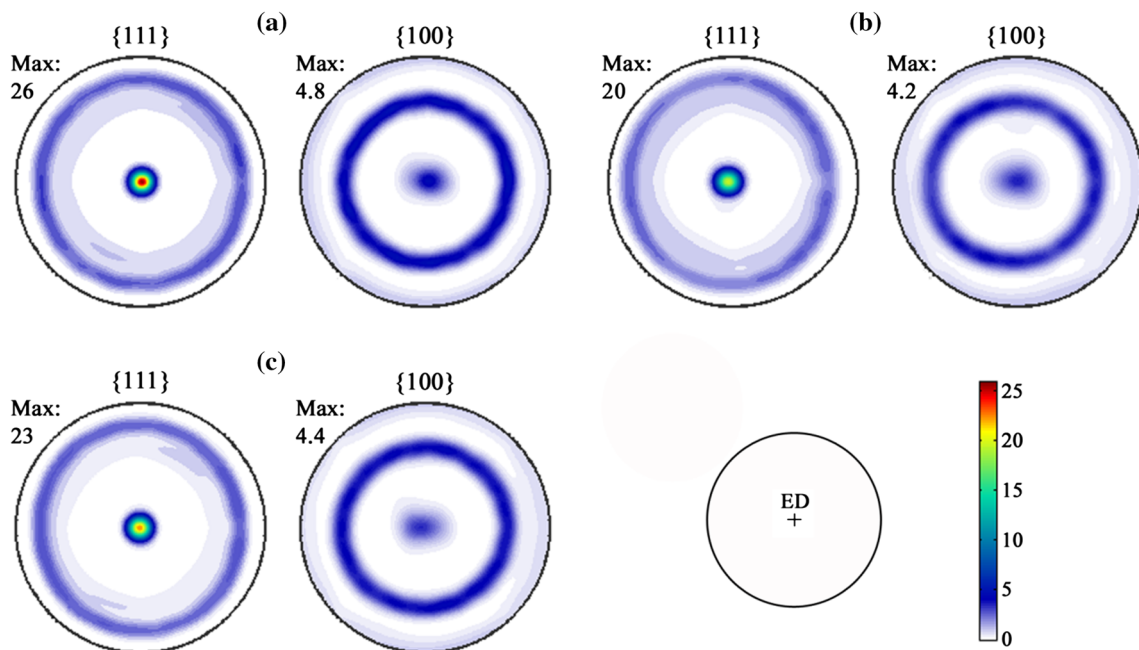

Figure 4 {111} and {100} pole figures (PFs) of **a** the pure Al bar, **b** the Al/GO composite and **c** the Al/CNT composite. The extrusion direction (ED) is perpendicular to the PFs.

Table 1 Volume fraction (within 15° with the extrusion direction) of Al grains associated with the <111> and <100> texture components and with random orientations

Material	<111>//ED (%)	<100>//ED (%)	Random orientations (%)
Pure Al	71.1	19.6	9.3
Al/GO	64.0	19.5	16.5
Al/CNT	69.2	17.8	13

deformed grains and the <001> fibre component corresponding to those grains obtained by recrystallisation during the extrusion process [20]. Adding carbonaceous materials results in a slight reduction in texture intensity compared with pure Al (Fig. 4a). This weakening effect appears to be more important for GO additions (Fig. 4b) than for CNTs additions (Fig. 4c).

For a more quantitative analysis of the weakening of the texture, the volume fraction of the <111> and <001> components were calculated (within 15 degrees tolerance) from the macrotexture data for the three materials (Table 1). The results show that the volume fraction of the <111> component is lower in the composites than in the unreinforced material, particularly in the Al/GO composite. However, the decrease in the volume fraction of deformed grains with <111>//ED promoted by the reinforcement additions does not result in an increase in the volume fraction of recrystallised grains with <001>//ED or cube-oriented grains, but in an increase in the volume fraction of grains with random orientations, especially for the Al/GO composite. This could be related to limited grain rotations around reinforcement agglomerations [21]. As a consequence of the formation around such agglomerations of deformation zones, where very high density of dislocations and strong lattice rotations are built up, grain rotations will be restricted [21, 22]. As a result, the grains in these regions cannot rotate to the same orientations as the rest of the matrix, resulting in a weaker texture [21]. This could explain the slight texture weakening in the composite materials relating to pure Al. However, since the degree of agglomeration and thus the extent of deformation zones is higher for CNTs than for GO, it could not explain why texture is weaker for the Al/GO than for the Al/CNT composite, which calls for another or an additional texture weakening mechanism. It could be related to the stabilisation of unusual texture components by retardation of grain growth. The cube texture is, due to the high growth rate of the cube-oriented rate, the most common recrystallisation texture for Al alloys

[20]. However, a recrystallisation process involving boundary pinning, more effective for GO than for CNTs, would restrict the preferential growth of the <001> component, enabling recrystallised grains with other orientations to grow and thus leading to weaker textures [23].

Interfaces and reinforcement structure

Raman spectroscopy was performed to characterise the structure of the reinforcements before and after they were incorporated in the Al matrix (Fig. 5). The Raman spectra as much of both the initial reinforcing materials and the composite materials display the first-order D and G bands, typically located at around 1335 and 1600 cm^{-1}, respectively [24]. The broad D and G bands as well as a D band that is of higher intensity than the G band (Table 2) are indicative of a high density of structural defects in the reinforcements [24]. Moreover, in the Al/CNT composite the band positions, especially the D band position, remain essentially invariant in comparison with those of the starting CNTs, but in the Al/GO composite there is a clear shift of the D band towards lower wavenumber and of the G band towards higher
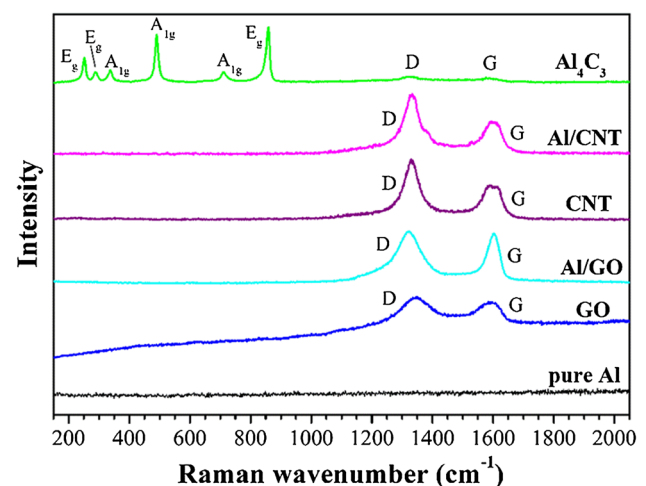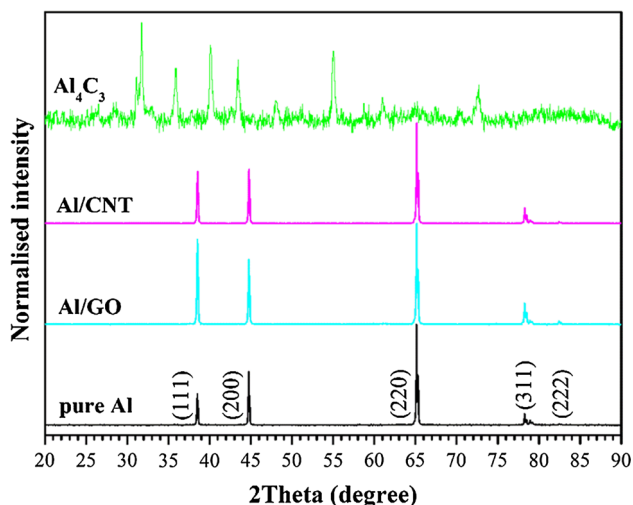

Figure 5 Raman spectra of the Al_4C_3 powder, the initial reinforcing materials, the composites and the pure Al bar.

Table 2 Position of the Raman D and G bands and the ratio of the band intensities (I_D/I_G) for the initial reinforcements and the composite materials

Material	Band position (cm^{-1})		I_D/I_G
	D band	G band	
GO	1344	1591	1.4
Al/GO	1321	1601	1.1
CNT	1330	1586	1.9
Al/CNT	1331	1590	2.1

wavenumber relative to the starting GO (Table 2). This is an evidence of the high instability of GO, both undergoing reduction and allowing the introduction of strain-induced defects in its structure during the composite fabrication [24, 25].

It is known that under high temperatures Al has high affinity to carbon-based materials and form carbides [17], which may be detrimental for the mechanical performance of the composite materials [6, 16]. As shown in Fig. 5, despite the apparently high presence of defects, which are preferential sites for carbide formation [16], no peaks of the Al_3C_4 phases are observed in the Raman spectra of composite materials, which suggests that no chemical reactions occurred between the reinforcements and the Al matrix. The absence of carbide in the interfaces between the Al matrix and the reinforcements is also apparent in the XRD patterns of the Al/GO and Al/CNT composites (Fig. 6), where peaks of the Al_3C_4 phases are not observed either.

Figure 6 XRD patterns of Al_4C_3 powder, the Al/CNT and Al/GO composites and the pure Al bar.

It is also possible to use polarised Raman spectroscopy to assess [26] the level of orientation of the reinforcements in the composites as shown in Fig. 7. The intensity of the D band was determined as a function of the angle between the direction of Raman laser polarisation and the extrusion direction. In both cases, the intensity peaks are a maximum at 0°, 180° and 360° and are a minimum at 90° and 270°. It can be seen that there is a much larger variation in the intensity with angle for the Al/GO than for the Al/CNT material, which indicates that the GO reinforcement is more highly aligned in the ED than the CNTs in the composites [26].

Mechanical properties

The average Vickers hardness (from 10 individual indentations) of the pure Al bar and the Al/GO and Al/CNT composites on sections perpendicular and parallel to the ED is plotted in Fig. 8. It is clear that GO additions strengthen the Al matrix, but CNT additions do not. So, while the additions of GO increase the Vickers hardness of the Al matrix by 12–14%, the additions of CNTs into the Al matrix have a negligible effect on microhardness. These results are, in principle, consistent with the relative mean grain sizes observed for the three materials (Fig. 3). It should be noted that the Vickers hardness values of the three materials are slightly higher on transversal (perpendicular to the ED) than on longitudinal (parallel to the ED) sections. This could be attributed to the elongated grain structure produced by extrusion, which results in an effective grain size smaller in the transversal rather than in the longitudinal sections.

Figure 9a illustrates typical examples of the engineering stress–engineering strain curves from the compressive tests performed along the ED on pure Al, Al/GO and Al/CNT samples. The work hardening rate, calculated as the slope of these curves at each strain, has been added as an inset. Figure 9b illustrates the average stress values (measured over 2 samples for pure Al, 5 samples for the Al/GO composite and 3 samples for the Al/CNT composite) for the three tested materials at different strains. Figure 9a shows that, during the first stages of plastic deformation, the work hardening rate is higher for the composite materials than for the unreinforced one, suggesting that reinforcing materials act as effective barriers for dislocations in the composites.
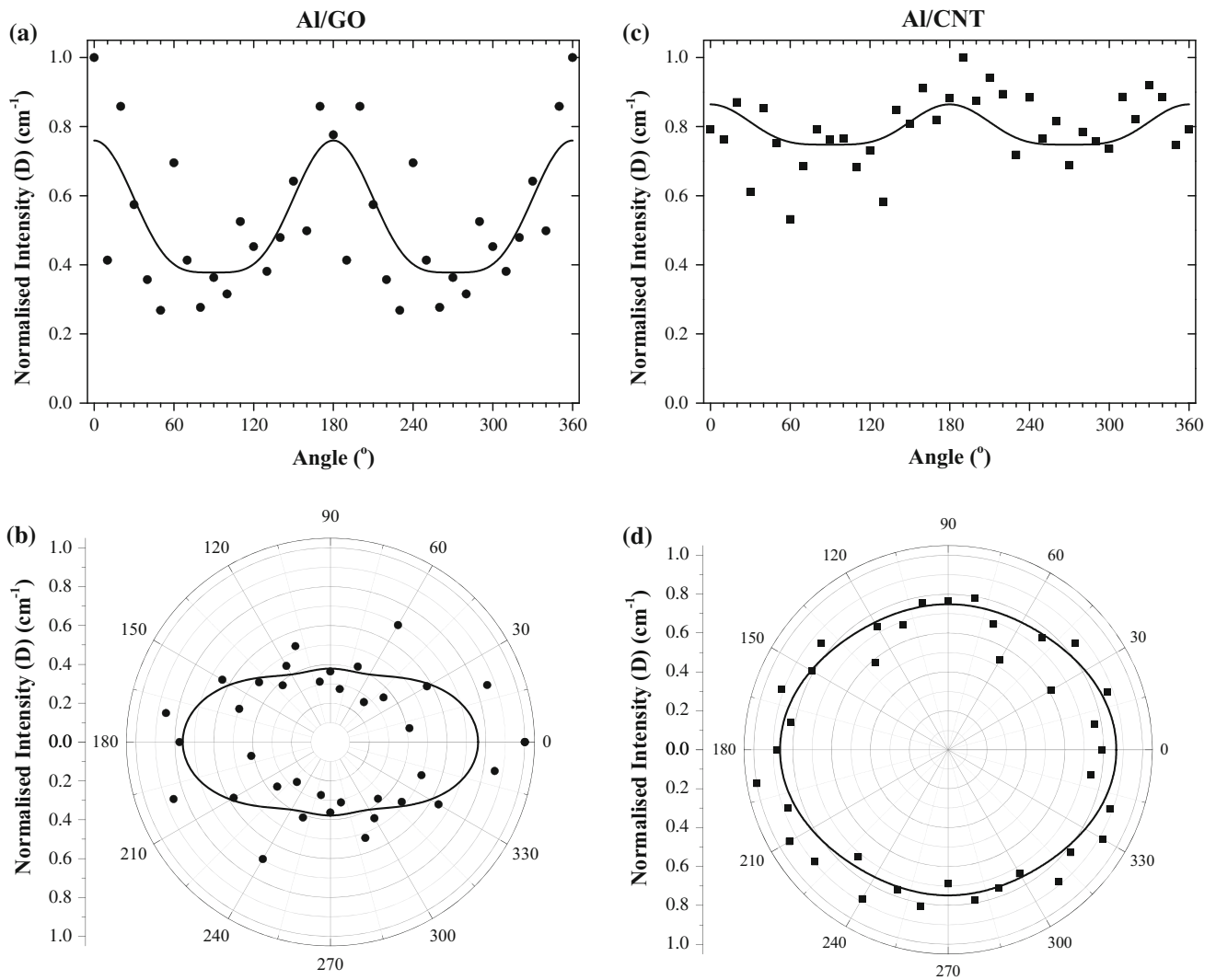
(a) Al/GO

(c) Al/CNT

(b)

(d)

Figure 7 Analysis of orientation of the GO and CNTs in the composites determined using Raman spectroscopy. Variation of the normalised intensity of the D band with the angle of rotation for **a** the Al/GO composite (*linear plot*), **b** the Al/GO composite (*circular plot*), **c** the Al/CNT composite (*linear plot*) and **d** the Al/CNT composite (*circular plot*).

In this case, during plastic deformation dislocations accumulate in the vicinity of the interfaces pinning each other and forming tangles, which decrease their mobility. Therefore, after the yield stress or elastic limit, an increase in stress is required to continue plastic deformation. Once the balance between the rates of dislocation generation and annihilation and thus the work hardening rate is similar and close to zero for the three materials (from about 10% engineering strain), the compressive stress is about 10% higher for the Al/GO composite than for pure Al and the Al/CNT composite (Fig. 9a,b). This is consistent with trend followed by hardness (Fig. 8), in turn,

consistent with the relative mean grain sizes observed for the three materials (Fig. 3). However, the average yield stress takes a value of 130 ± 9 MPa for pure Al, 134 ± 8 MPa for the Al/GO composite and 110 ± 10 MPa for the Al/CNT composite. Hence, as happens with hardness, the average yield stress of the Al/GO composite is slightly higher than that of pure Al, which is attributable to grain refinement, but it is lower for the Al/CNT composite than for pure Al despite the similarity of their mean grain sizes. This suggests that the mechanical behaviour of the present composites is not only determined by the grain size of the Al matrix.
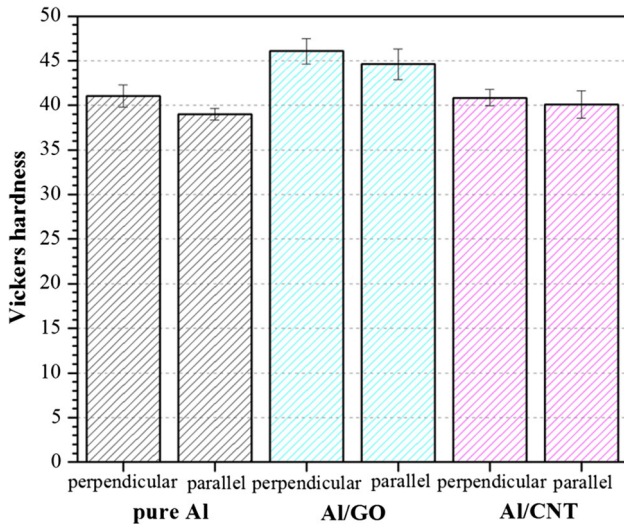
Figure 8 Average Vickers hardness of the pure Al bar and the Al/GO and Al/CNT composites.

Discussion

A deterioration of the mechanical properties observed has been previously reported for other metal matrix composites reinforced with carbonaceous materials. It has been usually related to a poor efficiency of load transfer from the matrix to the reinforcement during deformation, which is governed by factors such as the strength of the interfacial bonding between the matrix and the reinforcement and the dispersion of the reinforcement within the matrix. For example, owing to the formation of interfacial carbide, Bartolucci et al. [27] found a decreased tensile yield stress and hardness in an Al/

0.1 wt% graphene composite in comparison with pure Al, despite the fact that the composite exhibited a finer microstructure than pure Al. Kuzumaki et al. [28] observed a room temperature tensile yield stress slightly lower for the Al/5 vol% CNT and Al/10 vol% CNT composites than for pure Al as well as a slight difference in the mechanical properties between both composites. This was mainly attributed to a non-homogeneous dispersion of the nanotubes in the Al matrix. Salas et al. [29] reported a hardness decrease in Al matrix composites reinforced with CNTs as compared with pure Al. Moreover, this decrease in hardness, ascribed to the agglomeration of CNTs and a poor bonding between the Al matrix and the reinforcement, was shown to be higher with the increase in the volume fraction of CNTs.

In the Al/GO and Al/CNT composite studies, no carbides were observed at the interfaces between the matrix and the reinforcements (Figs. 5, 6). However, the absence of carbides does not ensure high-quality interfaces and therefore an effective load transfer across the phase matrix region. Moreover, a homogeneous distribution of reinforcement within the matrix is also essential to guarantee a high load transfer efficiency [6, 8, 12, 13, 15]. SEM (Fig. 1) and Raman mapping (Fig. 2) examinations on the present composites revealed a very poor dispersion of CNTs in the Al matrix. So, the reduced compressive yield stress of the Al/CNT composite relative to pure Al could be attributed to a poor efficiency of the load transfer caused by the large degree of agglomeration or clustering of the CNTs in the Al matrix. These results show that the strengthening effect of
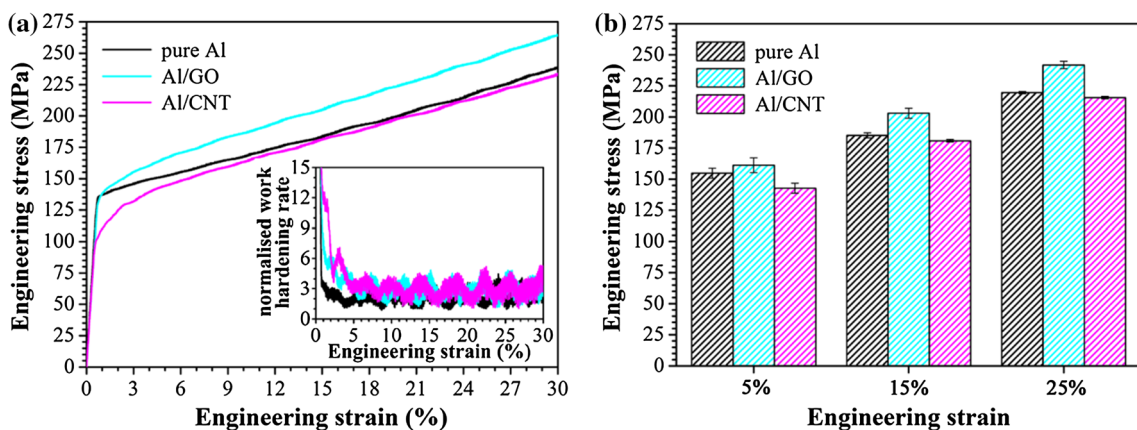

Figure 9 Compression tests results for the pure Al bar and the Al/GO and Al/CNT composites. **a** Typical engineering stress–engineering strain curves. The *inset* shows the corresponding normalised work hardening rate curves. **b** Average engineering stress at 5, 15 and 25% engineering strain.

carbonaceous materials is not only controlled by the metal matrix microstructure, but they are also largely dependent on the achievement of effective load transfer across the metal–reinforcement interface.

Conclusions

Two aluminium (Al) matrix composites reinforced with 0.5 wt% graphene oxide (GO) and 0.5 wt% carbon nanotubes (CNTs), respectively, were prepared by a combination of ball milling and hot extrusion. The microstructure, texture and mechanical behaviour of the composites compared with the unreinforced material as well as the interfacial reactions and the reinforcement structure were analysed.

It can be concluded that both reinforcing materials tend to disperse heterogeneously in the Al matrix, resulting in the formation of agglomerates at the grain boundaries (GBs), the extent of clustering being higher in the Al/CNT composite than in the Al/GO material. As a consequence, the Al/GO exhibits a more refined microstructure than pure Al due to the pinning effect of GO and, in turn, increased mechanical properties. On the contrary, the Al/CNT composite, with the same mean grain size as the unreinforced material, exhibits decreased compressive yield stress, attributable to a low efficient load transfer resulting from the large agglomeration degree of CNTs.

Finally, texture consists of the double <111> + <100> fibre, typical of extruded Al bars. Compared with pure Al, the intensity of this texture decreases with the addition of both carbonaceous materials due to the formation of deformation zones around the agglomerations. In addition, the pinning of GBs can contribute to restrict the preferential growth of certain orientations, leading to further texture weakening in the Al/GO composite.

Acknowledgements

Compliance with ethical standards

References

[1] Starke EA Jr, Staley JT (1996) Applications of modern aluminium alloys to aircraft. Prog Aerosp Sci 32:131–172

[2] Williams JC, Starke EA Jr (2003) Progress in structural materials for aerospace systems. Acta Mater 51:5775–5799

[3] Miller WS, Zhuang L, Bottema J, Wittebrood AJ, De Smet P, Haszler A, Vieregge A (2000) Recent development in aluminium alloys for the automotive industry. Mater Sci Eng A 280:37–49

[4] Li JL, Xiong YC, Wang XD, Yan SJ, Yang C, He WW, Chen JZ, Wang SQ (2015) Microstructure and tensile properties of bulk nanostructured aluminium/graphene composites prepared via cryomilling. Mater Sci Eng A 626:400–405

[5] Yan SJ, Dai SL, Zhang XY, Yang C, Hong QH, Chen JZ, Lin ZM (2014) Investigating aluminium alloy reinforced by graphene nanoflakes. Mater Sci Eng A 612:440–444

[6] Ibrahim IA, Mohamed FA, Lavernia EJ (1991) Particulate reinforced metal matrix composites: a review. J Mater Sci 26:1137–1156. doi:10.1007/BF00544448

[7] Miracle DB (2005) Metal matrix composites—from science to technological significance. Compos Sci Technol 65:2526–2540

[8] Mortensen A, Llorca J (2010) Metal matrix composites. Annu Rev Mater Res 40:243–270

[9] Ritchie RO (2011) The conflicts between strength and toughness. Nat Mater 10:817–822

[10] Mavhungu ST, Akinlabi ET, Onitiri MA, Varachia FM (2016) Aluminium matrix composites for industrial use: advances and trends. Procedia Manuf 7:178–182

[11] Xiong D-B, Cao M, Guo Q, Tan Z, Fan G, Li Z, Zhang D (2015) Graphene-and-copper artificial nacre fabricated by a preform impregnation process: bioinspired strategy for strengthening–toughening of metal matrix composite. ACS Nano 9:6934–6943

[12] Tjong SC (2013) Recent progress in the development and properties of novel metal matrix nanocomposites reinforced with carbon nanotubes and graphene nanosheets. Mater Sci Eng R 74:281–350

[13] Li Z, Guo Q, Li ZQ, Fan GL, Xiong DB, Su YS, Zhang J, Zhang D (2015) Enhanced mechanical properties of graphene (reduced graphene oxide)/aluminum composites with a bioinspired nanolaminated structure. Nano Lett 15:8077–8083

[14] Young RJ, Kinloch IA, Gong L, Novoselov KS (2012) The mechanics of graphene nanocomposites: a review. Compos Sci Technol 72:1459–1476

[15] Bakshi SR, Lahiri D, Agarwal A (2010) Carbon nanotube reinforced metal matrix composites: a review. Int Mater Rev 55:41–64

[16] Zhou W, Yamaguchi T, Kikuchi K, Nomura N, Kawasaki A (2017) Effectively enhanced load transfer by interfacial reactions in multi-walled carbon nanotube reinforced Al matrix composites. Acta Mater 125:369–376

[17] El-Ghazaly A, Anis G, Salem HG (2017) Effect of graphene addition on the mechanical and tribological behavior of nanostructured AA2124 self-lubricating metal matrix composite. Compos Part A Appl Sci Manuf 95:325–336

[18] Corrochano J, Hidalgo P, Lieblich M, Ibáñez J (2010) Matrix grain characterisation of powder metallurgy aluminium matrix composites reinforced with MoSi2 intermetallic particles. Mater Charact 61:1294–1298

[19] Corrochano J, Walker JC, Lieblich M, Ibáñez J, Rainforth WM (2011) Dry sliding wear behavior of powder metallurgy Al–Mg–Si alloy–MoSi$_2$ composites and the relationships with the microstructure. Wear 270:658–665

[20] Dillamore IL, Roberts WT (1965) Preferred orientation in wrought and annealed metals. Metall Rev 10:271–380

[21] Jiang X, Galano M, Audebert F (2014) Extrusion textures in Al, 6061 alloy and 6061/SiCp nanocomposites. Mater Charact 88:111–118

[22] Humphreys FJ, Kalu PN (1990) The plasticity of particle-containing polycrystals. Acta Metall Mater 38:917–930

[23] Hidalgo-Manrique P, Yi SB, Bohlen J, Letzig D, Pérez-Prado MT (2013) Effect of Nd additions on extrusion texture development and on slip activity in a Mg-Mn alloy. Metall Mater Trans A 44:4819–4829

[24] Li Z, Young RJ, Kinloch IA (2013) Interfacial stress transfer in graphene oxide nanocomposites. ACS Appl Mater Interfaces 5:456–463

[25] Poirier D, Gauvin R, Drew RAL (2009) Structural characterization of a mechanically milled nanotube/aluminium mixture. Compos Part A Appl Sci Manuf 40:1482–1489

[26] Li ZL, Young RJ, Kinloch IA, Wilson NR, Marsden AJ, Raju APA (2015) Quantitative determination of the spatial orientation of graphene by polarized Raman spectroscopy. Carbon 88:215–224

[27] Bartolucci SF, Paras J, Rafiee MA, Rafiee J, Lee S, Kapoor D, Koratkar N (2011) Graphene–aluminium nanocomposites. Mater Sci Eng A 528:7933–7937

[28] Kuzumaki T, Miyazawa K, Ichinose H, Ito K (1998) Processing of carbon nanotube reinforced aluminum composite. J Mater Res 13:2445–2449

[29] Salas W, Alba-Baena NG, Murr LE (2007) Explosive shock-wave consolidation of aluminum powder/carbon nanotube aggregate mixtures: optical and electron microscopy. Metall Mater Trans A 38:2928–2935